



New form for reduced modeling of soot oxidation: Accounting for multi-site kinetics and surface reactivity

Michael Frenklach

Department of Mechanical Engineering, University of California at Berkeley, Berkeley, California 94720-1740, USA



ARTICLE INFO

Article history:

Received 12 June 2018

Revised 12 August 2018

Accepted 20 December 2018

Keywords:

Soot oxidation
Reduced mechanisms
Surface reactivity
Particle dynamics

ABSTRACT

New formulation is introduced to model surface oxidation of soot particles. In the new development, the surface is represented by an arbitrary number of reactive sites and their physically-founded transformations. The latter are combined and integrated with gas-phase and particle-dynamics models. The surface reaction model defines two state properties and establishes a structural relationship between them that guides evolution of the surface. This new model form for the surface-chemistry led to close reproduction of shock-initiated oxidation of soot: CO profiles in two experiments performed at substantially different temperatures, 1990 and 2780 K, as well as CO production rates over a wide range of temperatures, 1652–3130 K, all without employing the parameter- α empiricism of the previous model formulation.

© 2018 The Combustion Institute. Published by Elsevier Inc. All rights reserved.

1. Introduction

Oxidation of soot is one of the constituent processes of soot particle dynamics [1]. It counters surface growth and ultimately is responsible for elimination of soot from the exhaust. A recent theoretical study [2] revealed that fundamental details of soot oxidation are more complex than assumed in current models. Moreover, the present numerical representation of the process in combustion modeling is inadequate to capture the new, emerging knowledge. This study reviews the shortcomings of the formalism presently used in modeling soot oxidation and introduces a new model form for a reduced representation of the processes identified in the detailed study [2].

Present models of soot oxidation consider OH and O₂ to be the primary oxidizers and express the former process through collision efficiency of OH with the particle surface [3] and the latter one either by an empirically-derived rate expression, most notably that of Nagle and Strickland-Constable (NSC) [4], or by a physically-based model, e.g., that of Appel et al. (ABF) [5].

The NSC expression has its origin in century-old experimental observations [6,7] of fast oxidation during a brief initial period followed by a slow-oxidation one. This phenomenon, which has been reproduced ever since (e.g., [8,9]), was explained by a two-reactive-site model, with more reactive, A, and less reactive, B, sites [6,7,10,11]. The NSC expression was developed by assuming first-order “thermal rearrangement” of A into B and oxidation of B forming Zachariah and co-workers [12] added thermally-activated

conversion of B into A. The parameters of these models were obtained by fitting the overall oxidation data.

In a quest for resolving the physical nature of surface sites, Frenklach suggested oxidation of soot surface by O₂ to be analogous to the oxidation of radical sites of polycyclic aromatic hydrocarbons (PAH) [13]. This chemical-analogy postulate has formed the foundation for a kinetic model [14]; one of its updated versions, ABF [5], has been widely used in modeling soot oxidation (and growth). The oxidation in that model is described by two processes: a single reaction step of O₂ with a surface radical, assumed to be in steady state, and the OH attack of a generic surface active site, following Neoh et al. [15].

Further exploration of the oxidation chemistry revealed a more complex behavior, involving multiple surface sites and an intricate coupling of the surface reaction kinetics to particle nanostructure (see [2] for review, discussion, and references). The identified principle reaction mechanism is formation of oxyradicals in reactions of surface radicals with O₂ and OH, decomposition of the oxyradicals that leads to the formation of imbedded five-member rings, and relatively slow oxidation of the latter by O atoms [2]. The kinetics of such a multi-site reaction network cannot be properly coupled to particle dynamics using the steady-state methodology of the earlier approach [14]. The present study develops and demonstrates a new way of accomplishing this.

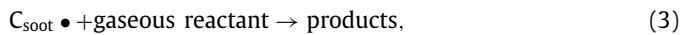
Part of the new development is a finer resolution of parameter α of the initial formulation [14], advancing formulation of surface reactivity in more physically-based terms. Hence, the presentation continues with a review of this subject matter; parameter α received a considerable attention in recent literature (see, e.g., [16–18]) and yet some of its aspects are not covered adequately.

E-mail address: frenklach@berkeley.edu

2. Modeling surface reactions, and parameter α

2.1. Physical model and numerical framework

The development of a detailed model for soot-particle surface reactions begun with the observation [13] that representing the particle surface as edges of polycyclic aromatic hydrocarbons (PAH) and applying the dominant reaction mechanism identified in the preceding modeling study [19],



reproduces the correct orders of magnitude for both soot oxidation by O_2 and soot growth by C_2H_2 . The latter has become known as HACA, an acronym given in [14] for the H-abstraction- C_2H_2 /Carbon-addition mechanism discovered in [19] (see [20] for further details).

The proposition of soot particle surface being comprised of PAH edges originated from and was consistent with the assumption of soot particle inception arising from PAH clustering [13,20,21]. Indeed, the two assumptions, PAH clustering into particles and HACA surface growth, link in very natural way the undergoing chemical reactions occurring at PAH edges: PAHs grow in size through a mechanism, such as HACA, and starting with a prescribed size, they begin to cluster, with the gas-phase reactions of these clustering PAHs evolving into surface reactions of the emergent particles.

Modeling of this physical system was enabled through parallel development of numerical methods: the growth of gas-phase PAH, up to an infinite size, was resolved via chemical lumping [22] and PAH clustering and particle dynamics via a method of moments that attained closure without a priori assumption of particle size distribution function (PSDF) [23]. Particle growth through mass deposition by surface chemical reactions was described by kinetic model (1)–(3) and the corresponding reaction rate expressions,

$$\text{reaction rate} = k_{g,s} C_g \chi_s S, \quad (4)$$

that couple the surface reaction kinetics with the dynamics of particle evolution [24]. In Eq. (4), $k_{g,s}$ is the per-site rate coefficient of reaction of gaseous reactant g with surface reactive site s , C_g is the concentration of gaseous reactant g , χ_s is the surface number density of sites s , and S is the soot particle surface area computed from the PSDF moments. Thus, the rate of the forward reaction (1) is given as

$$r_1 = k_1[\text{H}] \chi_{\text{C}_{\text{soot}}-\text{H}} S, \quad (5)$$

where $k_1[\text{H}]$ is the pseudo-first-order rate coefficient of reactions (1) and $\chi_{\text{C}_{\text{soot}}-\text{H}}$ is the number density of reactive C–H surface sites. The value of $\chi_{\text{C}_{\text{soot}}-\text{H}}$ was evaluated as

$$\chi_{\text{C}_{\text{soot}}-\text{H}} = \alpha \chi_{\text{nominal}}, \quad (6)$$

where χ_{nominal} is the nominal number density of possible C–H surface sites computed from purely geometric considerations and α is the fraction of these sites that undergo reaction, both properties discussed in the next section. The rest of the reaction rates of the (1)–(3) mechanism are

$$r_i = k_i[\text{G}_i] \chi_{\text{C}_{\text{soot}} \bullet} S, \quad (7)$$

where $\text{G}_i = \text{H}_2, \text{C}_2\text{H}_2, \text{O}_2$, and $\chi_{\text{C}_{\text{soot}} \bullet}$ is the number density of surface radicals, evaluated by assuming it to be in steady state and thus expressed through the established value of $\chi_{\text{C}_{\text{soot}}-\text{H}}$ [14].

2.2. Surface reactivity and parametrization

The nominal number density of the C–H surface sites, χ_{nominal} in Eq. (6), was evaluated in [14] from a geometric model of a soot particle whose surface is assumed to be composed of outward-looking PAH edges with PAH molecular moieties (or graphene flakes) assembled into turbostratic structures (not surface “covered with stacks of benzene rings” as misinterpreted in [16]). Estimating the area of a carbon surface site as 4.32 \AA^2 gives 2.3×10^{15} sites/cm² for the number density. Obviously, this estimate is an upper bound. It was known (and has continued to be confirmed [9,25,26]) from high-resolution electron microscopy [27–30] that not all PAHs (or PAH clusters) are positioned with their edges up but some (or many) with their basal planes up. In addition, not all PAH edge sites are reactive in the context of carbon growth and oxidation. The multiplier α , defined by Eq. (6) and often referred to as “parameter alpha”, accounts for the fraction of the nominal number density of surface sites that partake in carbon growth and oxidation reactions.

It was immediately found [14,31] that different flames required different values of α to reproduce experimental soot yields: namely, a single premixed laminar flame was able to be reproduced by adjusting α , but that value could not be transferred to another flame. Naturally, it was of interest to find a parametrization that could be applied more broadly.

From the known or presumed underlying physical picture, α has to be close to 1 at the initial phase, inception, when particles are forming from colliding PAHs and thus having their “surface” comprised essentially of PAH edges. The alignment of the PAH clusters with their basal planes up occurs with the increase in particle size and temperature. But then, after such alignment took place, there could be no “realignment back” with the decrease in temperature; surface PAHs continue to grow in a planar or somewhat curved manner [32]. Consistent with this mechanistic picture, values of α fitted to reproduce individual flames were found to correlate with the corresponding flame peak temperatures [31]. The observed correlation was summarized in [31] as

$$\alpha = \frac{1}{2} \left[1 + \tanh \left(\frac{a}{T_{\text{max}}} + b \right) \right], \quad (8)$$

where T_{max} is the peak flame temperature. This functional form assured α not to exceed its physical bounds, 1 and 0, and the fitted values of constants $a = 8168 \text{ K}$ and $b = -4.57$ provided a smooth asymptotical approach to unity at T_{max} below about 1500K, thereby covering the regime of particle inception in premixed laminar flames.

In a later study [5], the functional form of Eq. (8) was extended to include the dependence on particle size explicitly,

$$\alpha = \tanh \left(\frac{a(T)}{\log \mu_1} + b(T) \right), \quad (9)$$

where μ_1 is the first PSDF moment [24] and $a(T)$ and $b(T)$ became temperature-dependent parameters. The extended form, Eq. (9), expressed the desired physical trend of α decreasing with the increase in the particle size, while maintaining asymptotic approach to unity for the regime of particle inception (of lower particle sizes and lower temperatures). Parameters a and b , fitted for individual laminar premixed flames, exhibited a linear correlation with the flame peak temperature. Following this observation, parametric dependencies $a(T)$ and $b(T)$ were developed by fitting soot yields in eight premixed laminar flames, simultaneously, assuming that a and b are linear functions of local flame temperature. A follow-up study [33] slightly reparametrized $a(T)$ and $b(T)$, but retained the functional form of Eq. (9).

Kraft and co-workers [34] suggested expressing α in terms of soot particle age, A_p , which was tracked computationally in their

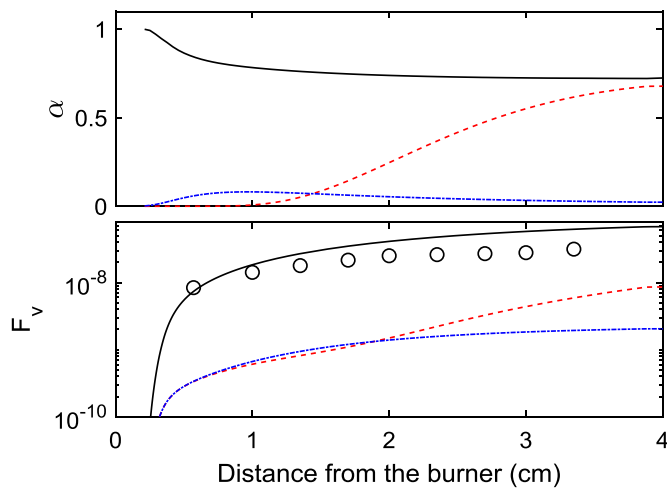


Fig. 1. Comparison of “parameter α ” expressions at the conditions of an atmospheric laminar premixed ethylene flame, JW1.69 [31, 36]; top panel – values of α computed by Eq. (9) as parametrized in [33] (solid black line), Eq. (11) [17] (dashed red line), and equation $\alpha = (6974.6/T_a^2) \exp(-88.06/T_a)$ [16] (dotted blue line); bottom panel – soot volume fraction: experimental data [36] (symbols) and computed (lines) with the model of Ref. [33] using the expressions of α displayed in the top panel. (For interpretation of the references to color in this figure legend, the reader is referred to the web version of this article.)

stochastic simulations. The developed correlation,

$$\alpha = 0.2 + 0.8 e^{(882 - 0.52T_{\max})A_p}, \quad (10)$$

was based on analysis of several premixed laminar flames, exhibiting behavior similar to that of Eq. (9) as parametrized in [5].

Dworkin and co-workers [16–18,35] devoted considerable effort on developing formulation for α applicable to modeling soot formation and oxidation in diffusion laminar flames. Veshkini et al. [16] suggested correlating α against thermal age, defined as the integral of the temperature that a soot particle experiences over its residence time, namely $T_a = \int T dt$. The latest parametrization originating from this effort [17] is of the form

$$\alpha = \left(\frac{T_{a,\max}}{T_a} \right)^{2.2} e^{2.4 \left(0.85 - \frac{T_{a,\max}}{T_a} \right)}, \quad (11)$$

where $T_{a,\max}$ is the thermal age at the point of maximum soot. While this expression exhibits a decrease in α with the increase in local flame temperature at later stages of particle evolution, it does not capture the inception-region behavior required for description of soot formation in premixed laminar flames. This is demonstrated in Fig. 1, which compares the different parametrizations of α in numerical simulations of an atmospheric premixed laminar flame of ethylene, designated as JW1.69 [31,36], one of the eight-flame set that served the basis for the development of Eqs. (8) and (9) [5,31,33]. The results displayed in Fig. 1 show that the expression developed for α with the laminar diffusion flames does not predict soot evolution in premixed laminar flames (and seemingly vice versa [16,17]). It is conceivable that an expression fitting both premixed and diffusion laminar flames could be developed, but then will such an expression be meeting other conditions, such as turbulent flames?

Irrespective of differences among above empirical formulations, all of them use global properties—temperature, particle size, or age—as surrogates for the atomistic state of soot particle surface. In the past three decades since the introduction of model (1)–(3), understanding of soot surface processes advanced to the level of detailed, sterically-resolved kinetics [2,32,37,38]. At the detailed atomistic resolution, modeling is able representing the surface processes as Markovian sequence of reaction events [39–41] with the

reaction outcome determined by an instantaneous state of the particle surface, thereby eliminating the need for empirical parameterization and tracking particle history. Yet, such models are computationally expensive for the use in numerical simulations of practical combustion systems. At the same time, as explained in the introduction, the nearly 30-year old approach based on model (1)–(3) does not have provisions to capture the current knowledge of soot surface chemistry. Motivated by these considerations, the objective of the present study is to advance reduced formulation of soot kinetics to a higher level of atomistic resolution, effective in representing multi-site reaction mechanisms for practical applications.

3. Essential features of the new model form

One of the core elements of the new development is representation of soot surface by an arbitrary number of reactive sites and their physically-founded transformations. The latter are combined with the gas-phase reaction model. This integration offers flexibility in selecting a surface reaction submodel, its form (e.g., detailed or empirical), parameterization, and coupling to the particle dynamics, as exemplified with the present development. It naturally accounts for the effects of gaseous species on the state of the surface and, vice versa, the influence of surface reactions on the concentrations of gaseous species. The surface oxidation rate is obtained directly from the surface-reaction rates and is used in particle-dynamics part of the combined model. The properties computed by the particle-dynamics submodel are used in regulating the surface-reaction kinetics.

Another core component of the new development is accounting for the surface steric effects via a given state of the surface, namely, by instantaneous number densities of surface sites, thereby eliminating the need for empirical parametrization of surface reactivity. In doing so, the surface reactivity is determined in an identical manner for any reactive process, such as oxidation, growth, and thermal annealing.

While the new formulation can be applicable to both soot growth and soot oxidation, it starts here with the oxidation. First, the improved knowledge of graphene-edge oxidation reactions [2], which motivated the present study, rests in the fact that the oxidation is controlled by not just oxidation of surface radicals but also, and critically, by the formation of embedded five-membered rings, the process that cannot be properly captured by the single steady-state of the generic surface radical of the old formalism. Second, experimental data available for model validation is more direct in the case of oxidation as compared to growth. Indeed, the rate of growth is determined by deconvolution of optical or mass measurements of particle cloud, whose evolution is affected also by particle nucleation, coagulation, and fragmentation. The rate of oxidation, on the other hand, can be inferred from more direct measurements of carbon oxide products, and starting with a priori prepared soot particle sample eliminates the dependence on the details of particle nucleation and surface growth. The experiment data chosen for the present analysis were collected at conditions that allow one to make further simplifying assumption. Hence, the presentation continues with the description of those data and conditions.

4. Selected experimental data

Following the previous numerical study [2], the shock-tube data collected by Roth et al. [42] on soot particle oxidation were chosen for the present analysis. With this technique, a homogeneous mixture is heated instantaneously to high temperatures and reacts for a relatively short period of time, thus creating a gaseous environment for soot oxidation that is better understood in terms of elementary chemical reactions and that is amenable to more detailed

quantitative modeling [2]. The oxidative environment utilized in these experiments was made of H₂–O₂–Ar mixtures, thus providing one of the simplest systems, with better-known kinetics and without sources of carbon that would otherwise complicate the analysis with the surface growth. Having no carbon in the oxidative gaseous mixture allowed Roth et al. to measure soot oxidation rate directly, by laser absorption of CO and CO₂. The large amounts of H₂, included in the gaseous mixtures, alleviated possible influence of extraneous sources of H atoms [2].

A sample of carbonaceous particles, prepared in a specially-designed aerosols generator [43], was dispersed in the shock tube prior to reaction. The initial sample was of a commercial grade, lamp black 101 of Degussa. While there are clear differences between carbon black produced in commercial flame reactors and soot formed in engines or forest fires [44,45], the carbonaceous particles formed in laboratory flames from controlled fuel mixtures, composed of pure hydrocarbons and free of mineral matter, have primary-particle structure similar to that of carbon black (e.g., [25,29,46,47]), the fact underlying the frequent use of both materials interchangeably in fundamental soot studies (e.g., [48]), including those of Roth and co-workers [42], as well as utilization of the knowledge gained from soot studies for carbon black processes (e.g., [49,50]). These facts and consideration that the present modeling study is focused primarily on the structural aspects associated with the aromatic composition of the carbonaceous particle serve as justification for the use of Roth et al.'s experimental observations for comparison with model predications in the present study.

The properties of the injected particle cloud were determined by multiple-wavelength laser-light absorption. For the experiments used in the present study, Roth et al. [42] reported the most probable diameter of the injected particles, $D_{pm} = 110$ nm, and the particle surface area per cm³ of suspension, a_p , specified for individual shock-tube experimental runs. As no further information on the initial particle cloud was reported, its additional properties were computed here through PSDF estimated as follows. The PSDF was assumed, following Roth and co-workers [43], to be lognormal of particle diameter, D_p ,

$$n_d(D_p) = \frac{N_{total}}{\sqrt{2\pi} D_p \ln \sigma_g} e^{-\frac{(\ln D_p - \ln D_{pg})^2}{2(\ln \sigma_g)^2}}, \quad (12)$$

and quantified by specifying its three parameters: geometric mean diameter, D_{pg} , geometric standard deviation, σ_g , and the total number of particles, N_{total} , [51]. The geometric mean was evaluated from the reported value of $D_{pm} = 110$ nm through the known relationship (e.g., [52])

$$\ln D_{pg} = \ln D_{mode} + (\ln \sigma_g)^2. \quad (13)$$

The geometric standard deviation, σ_g , was assigned a value of 1.6, based on the analysis performed on the same or similar carbon-black grades [53,54]. The value of N_{total} was then computed from

$$a_p = \int_0^{\infty} \pi D_p^2 n_d(D_p) dD_p. \quad (14)$$

Defined in this manner PSDF, Eq. (12), was used to compute the initial values of PSDF moments, discussed in Section 5.2.

5. Model

The numerical model is a single system of ordinary differential equations (ODE) that includes three subsystems: gas-phase reactions, surface reactions, and particle dynamics. The details of these submodels and their integration are presented in the following subsections.

5.1. Gas phase

Similar to the prior study [2], the kinetics of the gaseous H₂–O₂–Ar mixtures used in Roth et al.'s experiments [42] was modeled by an optimized H₂–O₂ reaction model of You et al. [55], documented in the PrIME Data Warehouse [56], augmented by reaction $\text{CO} + \text{OH} \rightleftharpoons \text{CO}_2 + \text{H}$ with the rate coefficient recommended by Baulch et al. [57].

5.2. Particle dynamics

The conditions of Roth et al.'s experiments [42] have characteristics that allow us to make simplifying assumption, detailed as follows. Notwithstanding that the lamp black has a broad particle-size distribution, its mode is rather large, $D_{pm} = 110$ nm, and consequently most particles of the cloud are relatively large (e.g., the two-sigma interval, $\ln D_{pm} \pm 2 \ln \sigma_g$, contains 93 % of the particles). On this basis, we can assume coagulation/aggregation to be relatively small. The observations of Roth et al. [42] corroborate this further by reporting a rather small change in a most probable diameter of the primary particles (80 nm) to that of agglomerates (110 nm) forming during particle dispersion. Considering further that most initial particles are of larger sizes and that their oxidation takes place for a short period of time implies a small extent of particle oxidation and hence a small change in particle size. The latter is confirmed in the present simulations, as presented in Section 6. If particle size does not change appreciably during oxidation, then the extent of particle fragmentation and of particle complete burnout should be small as well.

Given the above arguments, particle dynamics under Roth et al.'s experimental conditions can be modeled neglecting particle coagulation, aggregation, fragmentation, and complete burnout. Under these assumptions, a simple variant of the method of moments is proposed here.

In the method of moments (MoM), a particle system is described in terms of PSDF moments,

$$M_r = \sum_{i=1}^{\infty} m_i^r N_i, \quad (15)$$

where M_r is the r th PSDF moment, and m_i and N_i are the mass and number density, respectively, of the i th particle class. In the prior discrete MoM derivation [58], the particle classes are defined by a preset, unchanging set of masses; i.e., in differentiating Eq. (15), m_i 's are considered constant,

$$\frac{dM_r}{dt} = \sum_{i=1}^{\infty} m_i^r \frac{dN_i}{dt}. \quad (16)$$

This approach enables straightforward formulation of particles coagulation [23] and aggregation [59,60].

Without the need to account for particle coagulation, a simpler approach is emerged by classifying particles by their initial identity. In other words, given an initial set of N_i particles, we consider that N_i 's are now constants and m_i 's are changing due to surface processes; i.e., by differentiating Eq. (15), we get

$$\frac{dM_r}{dt} = \sum_{i=1}^{\infty} \left(r m_i^{r-1} \frac{dm_i}{dt} N_i \right). \quad (17)$$

The oxidation rate of an individual particle is

$$\frac{dm_i}{dt} = -k_s S_i, \quad (18)$$

where S_i is the surface of i th-class particle and k_s is the surface oxidation rate (in g cm⁻² s⁻¹). Assuming particles are spherical with density $\rho = 1.86$ g cm⁻³ [42], we rewrite Eq. (18) as

$$\frac{dm_i}{dt} = -k_m m_i^{2/3}, \quad (19)$$

where

$$k_m = k_s \pi \left(\frac{6}{\pi \rho} \right)^{2/3}. \quad (20)$$

Multiplying Eq. (19) by N_i and summing up, we get

$$\sum_{i=1}^{\infty} \left(\frac{dm_i}{dt} N_i \right) = \sum_{i=1}^{\infty} (-k_m m_i^{2/3} N_i); \quad (21)$$

recalling that N_i is time independent and exchanging the order of summation and differentiation on the left-hand side of Eq. (21) gives

$$\frac{d}{dt} \left(\sum_{i=1}^{\infty} m_i N_i \right) = -k_m \sum_{i=1}^{\infty} m_i^{2/3} N_i \quad (22)$$

and recalling the definition (15), we obtain

$$\frac{dM_1}{dt} = -k_m M_{2/3}. \quad (23)$$

To determine $M_{2/3}$, appearing on the right-hand side of Eq. (23), we start with Eq. (17) for $r=2/3$,

$$\frac{dM_{2/3}}{dt} = \sum_{i=1}^{\infty} \left(\frac{2}{3} m_i^{-1/3} \frac{dm_i}{dt} N_i \right), \quad (24)$$

and substitute dm_i/dt by Eq. (19),

$$\frac{dM_{2/3}}{dt} = -\frac{2}{3} k_m \sum_{i=1}^{\infty} m_i^{1/3} N_i = -\frac{2}{3} k_m M_{1/3}. \quad (25)$$

The equation for $M_{1/3}$, appearing on the right-hand side of Eq. (25), is obtained in a similar manner,

$$\frac{dM_{1/3}}{dt} = -\frac{1}{3} k_m \sum_{i=1}^{\infty} m_i^{-2/3} m_i^{2/3} N_i = -\frac{1}{3} k_m \sum_{i=1}^{\infty} N_i = -\frac{1}{3} k_m M_0. \quad (26)$$

The 0th moment, M_0 , appearing on the right-hand side of Eq. (26), is the total number of particles, N_{total} , as follows from Eq. (15). Since N_i 's are assumed to remain constant, so will be N_{total} , with its value specified by Eq. (14). With M_0 known, we attain the exact closure of the MoM equations, consistent with the analysis of Hulburt and Katz [61].

Summarizing the final results, we get

$$\begin{aligned} \frac{dM_0}{dt} &= 0 \\ \frac{dM_{1/3}}{dt} &= -\frac{1}{3} k_m M_0 \\ \frac{dM_{2/3}}{dt} &= -\frac{2}{3} k_m M_{1/3} \\ \frac{dM_1}{dt} &= -k_m M_{2/3} \end{aligned} \quad (27)$$

Solution of Eq. (27) provides time-dependent soot-particle properties, like mean particle diameter

$$\langle D_p \rangle = \frac{\sum_{i=1}^{\infty} D_{p,i} N_i}{N_{\text{total}}} = \frac{\sum_{i=1}^{\infty} \left(\frac{6 m_i}{\pi \rho} \right)^{1/3} N_i}{\sum_{i=1}^{\infty} N_i} = \left(\frac{6}{\pi \rho} \right)^{1/3} \frac{M_{1/3}}{M_0} \quad (28)$$

and surface area of a unit-volume of the particle ensemble

$$S = \sum_{i=1}^{\infty} S_i N_i = \sum_{i=1}^{\infty} \pi \left(\frac{6 m_i}{\pi \rho} \right)^{2/3} N_i = \pi \left(\frac{6}{\pi \rho} \right)^{2/3} M_{2/3}. \quad (29)$$

Such relationships are also used to obtain the initial conditions for Eq. (27), evaluating the initial mass moments, $M_{r,0}$, from the size moments of the initial lognormal distribution, Eq. (12),

$$M_{r,0} = \left(\frac{\pi \rho}{6} \right)^r \int_0^{\infty} D_p^{3r} n_d(D_p) dD_p. \quad (30)$$

The value of k_m , appearing in Eq. (27), is specified by

$$k_m = \frac{r_{\text{oxid}}}{M_{2/3}}, \quad (31)$$

which follows from the last of Eq. (27) recalling from Eq. (15) that M_1 is the total particle mass. The value of the mass oxidation rate, r_{oxid} , is established in the surface-kinetics part of the model, described next.

5.3. Surface reaction model

The surface submodel is the key and defining part of the new formalism. It commences with composition of a set of surface reaction steps. Such a set, assembled for the present study, is presented in Table 1. Its construction was based on the results of the detailed, sterically-resolved simulations and analysis of soot oxidation [2], which follows the direct, Eiley-Rideal surface kinetics as the previous studies [62].

All reaction steps in Table 1 are first or pseudo-first order with respect to surface sites, and their abundances are expressed in the units of mol/cm³. Adding this reaction set to the gas-phase one and solving the combined ODE system accounts in a direct manner for the influence of gaseous species on surface processes and, vice versa, for the impact of the surface reactions on the gas-phase composition. Also, the rate of CO production in surface reactions establishes the oxidation rate term, r_{oxid} in Eq. (31), for the particle-dynamics part of the model, Eq. (27),

$$r_{\text{oxid}} = 12 (r_{S4} + r_{S6} + r_{S8} + 2r_{S9}), \quad (32)$$

where r_{S4} , r_{S6} , r_{S8} , and r_{S9} are the rates (in units of mol cm⁻³ s⁻¹) of Reactions S4, S6, S8, and S9, respectively, and 12 is the atomic weight of the carbon atom.

The new model considers multiple surface reactive sites: arm-chair, C_A , zigzag, C_Z , their radicals and oxides, and embedded five-member rings, C_{R5} , as contrasted with the single “generic” C_{soot} of the previous model [5,14]. The site multiplicity is motivated by the new knowledge of the surface chemistry (see [2,32] and literature cited therein) and, specifically to the present study, by the need to account for the multi-step kinetics of the oxidation [2].

Reaction steps (S1)–(S8) in Table 1 encapsulate reactive chemistry of oxidation: formation and disappearance of surface radicals, formation of surface oxyradicals, their decomposition to gaseous carbon monoxide, CO, and surface five-member rings, C_{R5} , and oxidation of the latter by O atoms. Notation “– C_A -H” appearing on the right-hand side of reaction equations (S4) and (S6) symbolizes that an additional, neighboring C_A -H site is removed during the formation of the five-member ring, C_{R5} . Reaction (S9) represents thermal desorption of C_2H_2 and its subsequent oxidation in the gas phase to 2 CO + H₂. The reaction equation expresses in this case the reaction stoichiometry; its reaction rate, r_{S9} , is assigned half of $r_{S4} + r_{S6} + r_{S8}$, so that the rate of CO production through the C_2H_2 thermal desorption, represented by reaction (S9), is the same as the rate of CO formation in all the oxidation channels, represented by reaction steps (S4), (S6), and (S8). This assignment follows the results observed in the sterically-resolved simulations [2].

Reaction steps (S10)–(S16) capture reactions occurring on inner zigzag sites, those that do not undergo oxidation [73]. Of those, only reactions (S10) and (S11) were found to have an influence, albeit very small, at the simulated here conditions. The rest were

Table 1
Surface oxidation reaction model.

	Surface reaction	Rate coefficient (units mol/cm ³ , s, K)	Source
S1	C _A -H + H ⇌ C _A • + H ₂	forward 6.09 × 10 ⁷ T ^{1.85} e ^{-7448/T} reverse 1.07 × 10 ⁴ T ^{2.65} e ^{-2796/T}	Per-site, armchair [63]
S2	C _A • + H ⇌ C _A -H	3.26 × 10 ¹³ T ^{0.17}	High-pressure-limit 2-naphthyl + H [64]
S3	C _A • + O ₂ ⇌ C _A -O + O	1.29 × 10 ¹⁴ e ^{-1812/T}	High-pressure-limit 2-naphthyl + O ₂ [65, 66]
S4	C _A -O → C _{R5} + CO - C _A -H	6.42 × 10 ¹⁰ T ⁴ e ^{-29183/T}	High-pressure-limit, phenanthryl [67]
S5	C _A -H + OH ⇌ C _A • + H ₂ O	3.89 × 10 ³ T ^{2.683} e ^{-369/T}	1/6 k _{benzene+OH} [68]
S6	C _A • + OH → C _{R5} + CO - C _A -H	1.00 × 10 ¹⁴	[69]
S7	C _A -H + O ⇌ C _A -O + OH	2.40 × 10 ¹² e ^{-2328/T}	1/6 k _{benzene+O} [70]
S8	C _{R5} + O → Δ _A C _A -H + Δ _Z C _Z -H + CO	3.54 × 10 ¹¹ T ^{0.505} e ^{-306/T}	[2] (k _{S104})
S9	C _{R5} + O ₂ → Δ _A C _A -H + Δ _Z C _Z -H + 2CO + H ₂	r _{S9} = (r _{S4} + r _{S6} + r _{S8})/2	see text
S10	C _Z -H + H ⇌ C _Z • + H ₂	forward 9.80 × 10 ⁷ T ^{2.65} e ^{-8039/T} reverse 1.60 × 10 ⁴ T ^{2.63} e ^{-2137/T}	Per-site, zigzag [63]
S11	C _Z • + H ⇌ C _Z -H	4.86 × 10 ¹³ T ^{0.13}	High-pressure-limit 1-naphthyl + H [64]
S12	C _Z -H + OH ⇌ C _Z • + H ₂ O	3.89 × 10 ³ T ^{2.683} e ^{-369/T}	k _{S12} = k _{S5}
S13	C _Z • + O ₂ ⇌ C _Z -O + O	9.40 × 10 ¹³ e ^{-1771/T}	1-naphthyl + O ₂ [71]
S14	C _Z -O + H ⇌ C _Z -OH	4.34 × 10 ¹⁴ e ^{-984/T}	[69] (S69 in [2])
S15	C _Z • + OH ⇌ C _Z -OH	1.47 × 10 ¹⁴ e ^{-632/T}	[69] (S59 in [2])
S16	C _Z -OH + H ⇌ C _Z • + H ₂ O	2.00 × 10 ¹⁴ e ^{-2670/T}	[72] (S89 in [2])

added to test possible effects on gaseous O/OH/O₂ concentrations due to surface-catalyzed interconversions, referred to as the regeneration mechanism [71]. Similarly to the outcome of the prior tests [62], the impact of the regeneration mechanism was found to be insignificant. Nonetheless, reactions (S12)–(S16) were retained in the present model rendering a test option and can be removed if no significant impact is revealed.

One of the key processes in the mechanism is step (S8), oxidation of embedded five-membered rings by atomic oxygen. While rate limiting [2], it serves two additional tasks in the reduced model. First, reproduction of the initial surface sites, C_A-H and C_Z-H, accomplishes linear lumping [22] of the PAH reduction in size. Second, the stoichiometric split between the two sites, armchair and zigzag, aims at capturing the steric nature of the reaction outcome. These two features are also present in Reaction (S9). The mechanistic reasoning for the split will be discussed in Section 8; here, we continue with the model formulation.

Recovery of the sterically-driven kinetics in the reduced model is attained by employing two *state* properties: fraction of surface reactive sites, α, and zigzag fraction of the reactive sites, ζ. To retain harmony with the past work [14], I will keep the original definition of α given by Eq. (6). However, now it does not require parameterization, the kind described in Section 2, but its instantaneous value is expressed in terms of state variables, surface site concentrations, namely,

$$\alpha = \frac{\sum_i [C_{\text{reactive},i}]}{\sum_j [C_{\text{surface},j}]} = \frac{A + Z}{\chi_{\text{nominal}}} \quad (33)$$

where, for the present model in Table 1,

$$A = \sum_n [C_{A_n}] = [C_{A-H}] + [C_{A\bullet}] + [C_{A-O}] + [C_{R5}] \quad (34)$$

is the sum of all armchair site concentrations, and

$$Z = \sum_m [C_{Z_m}] = [C_{Z-H}] + [C_{Z\bullet}] + [C_{Z-O}] + [C_{Z-OH}] \quad (35)$$

is the sum of all zigzag site concentrations; the nominal number density of surface sites appearing in the denominator of Eq. (33) is obtained as

$$\chi_{\text{nominal}} = \frac{\chi_s}{N_{Av}} \pi \left(\frac{6}{\pi \rho} \right)^{2/3} M_{2/3}, \quad (36)$$

where $M_{2/3}$ is the instantaneous value of the 2/3-rd moment, obtained from solution of Eq. (25), and N_{Av} is the Avogadro number. Property ζ, the zigzag fraction of the reactive sites, is expressed

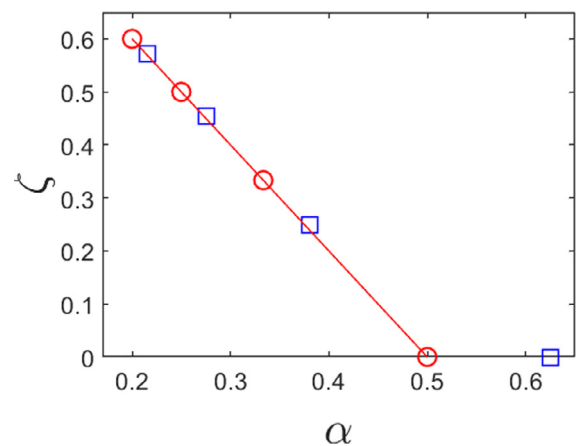


Fig. 2. Fraction of zigzag sites, ζ, versus fraction of reactive sites, α: red circles, coronene series; blue squares, pyrene series; red line, linear fit of the coronene series, ζ = 1 - 2α. (For interpretation of the references to color in this figure legend, the reader is referred to the web version of this article.)

in a manner similar to α, as a ratio of instantaneous surface-site concentrations,

$$\zeta = \frac{\sum_m [C_{Z_m}]}{\sum_i [C_{\text{reactive},i}]} = \frac{Z}{A + Z}. \quad (37)$$



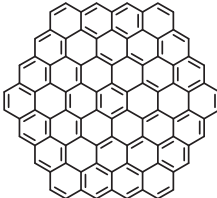
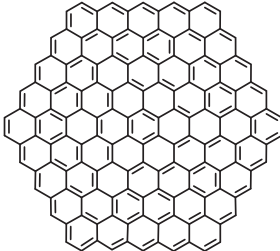
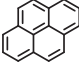
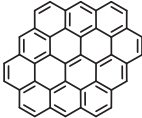

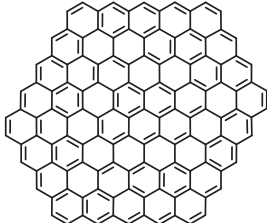
Stoichiometric coefficients Δ_A and Δ_Z of the armchair and zigzag product sites in Reactions (S8) and (S9) are assumed to be functions of α and ζ, and their values can be either integer or fractional numbers. Undoubtedly, development of these dependencies calls for challenging experimental and theoretical endeavors. At the present state of knowledge and for the rather small extent of particle oxidation (as confirmed in Section 6 for the experiments considered in the present analysis), the following parametrization was found compelling.

Let us begin by considering α and ζ values of two homologous PAH series, coronenes and pyrenes, summarized in Table 2. The ζ-vs-α relationship, displayed in Fig. 2, appears to follow a linear relationship,

$$\zeta = 1 - 2\alpha. \quad (38)$$

This simple relationship is exact for the coronene series and closely approximates the pyrene series, with the exception of pyrene itself, whose oxidation or pyrolysis should lead to rapid dissolution.

Table 2
Coronene and pyrene series.

Structure	Formula	α	ζ
coronene series			
	$C_{24}H_{12}$	$\frac{12}{24}$	$\frac{0}{12}$
	$C_{54}H_{18}$	$\frac{18}{54}$	$\frac{6}{18}$
	$C_{96}H_{24}$	$\frac{24}{96}$	$\frac{12}{24}$
	$C_{150}H_{30}$	$\frac{30}{150}$	$\frac{18}{30}$
pyrene series			
	$C_{16}H_{10}$	$\frac{10}{16}$	$\frac{0}{10}$
	$C_{42}H_{16}$	$\frac{16}{42}$	$\frac{4}{16}$
	$C_{80}H_{22}$	$\frac{22}{80}$	$\frac{10}{22}$
	$C_{130}H_{28}$	$\frac{28}{130}$	$\frac{16}{28}$

Let us assume, as a postulate, that the evolution of surface sites, on average, follows the $\zeta(\alpha)$ relationship, and assume further, for the present study, that this relationship is $\zeta = 1 - 2\alpha$. The rationale for this proposition is discussed in Section 8. Now, equipped with the postulate, we continue with the development of the armchair-zigzag stoichiometry.

From the conservation of mass, we have

$$\Delta_A + \Delta_Z = 2, \quad (39)$$

as removal of the outer carbon atom due to oxidation of the embedded five-member ring in Reaction (S8) and desorption of a chemisorbed C_2H_2 in Reaction (S9) each leaves behind two reactive surface sites, armchair and/or zigzag. Following the introduced above postulate, the split between armchair and zigzag should maintain the overall, global relationship between α and ζ , Eq. (38). Differentiating Eq. (38) with respect to time, while recalling definitions of α and ζ given by Eqs. (33) and (37),

$$\left(\frac{Z}{A+Z}\right)' = -2\left(\frac{A+Z}{\chi_{\text{nominal}}}\right)', \quad (40)$$

we get

$$\frac{Z'(A+Z) - Z(A+Z)'}{(A+Z)^2} = -2\frac{(A+Z)'\chi_{\text{nominal}} - (A+Z)\chi'_{\text{nominal}}}{\chi_{\text{nominal}}^2}, \quad (41)$$

which after rearrangement takes the form

$$Z' - (\zeta - 2\alpha)(A+Z)' = 2\alpha^2 \chi'_{\text{nominal}}. \quad (42)$$

Exact reproduction of reactive sites, as part of linear lumping, leaves the total number of them unchanged and hence

$$(A+Z)' = 0. \quad (43)$$

Substituting Eq. (43) into Eq. (42) and expressing χ'_{nominal} by differentiation of Eq. (36),

$$\frac{dZ}{dt} = \frac{\chi_s}{N_{Av}} \pi \left(\frac{6}{\pi \rho}\right)^{2/3} \frac{dM_{2/3}}{dt}, \quad (44)$$

results in

$$(r_{S8} + r_{S9})\Delta_Z = 2\alpha^2 \frac{\chi_s}{N_{Av}} \pi \left(\frac{6}{\pi \rho}\right)^{2/3} \frac{dM_{2/3}}{dt}. \quad (45)$$

Eq. (45) defines the production rate of zigzag sites in Reactions (S8) and (S9). Combining Eqs. (45) and (39) defines the corresponding rate of armchair sites,

$$(r_{S8} + r_{S9})\Delta_A = 2(r_{S8} + r_{S9}) - 2\alpha^2 \frac{\chi_s}{N_{Av}} \pi \left(\frac{6}{\pi \rho}\right)^{2/3} \frac{dM_{2/3}}{dt}. \quad (46)$$

Eqs. (45) and (46) thus establish the stoichiometric split between the armchair and zigzag sites.

5.4. Implementation

Time evolution of all state variables—gaseous species concentrations, surface site number densities, and moments of particle mass distribution—were obtained by numerical solution of the complete ODE system under adiabatic isochoric constraints, employing the Matlab ode15s solver [74], with its integration tolerance parameters set at RelTol = 1×10^{-5} and AbsTol = 1×10^{-20} . The thermodynamic data were taken from [75]. The particle temperature was assumed to be equal to that of the ambient gas, as typical for shock-tube analysis, since particle radiation losses are negligible [76].

6. Numerical results

The introduced above model was tested on the experimental data collected by Roth et al. [42] in shock-tube oxidation of soot particles. The motivation for focusing on these data was presented in Section 4. The first series of tests was performed on one particular experiment, the one that was extensively scrutinized in the prior detailed, sterically-resolved modeling study [2]; this selected experiment is in the middle of the temperature range studied by Roth et al. and is specified in most detail, with the explicit set of experimentally observed concentrations of gaseous CO, displayed in Fig. 7 of Roth et al. [42]. Like in the prior detailed study [2], the present modeling with the reduced model of Section 5 had its objective of matching the reported experimental CO profile.

The experimental gas-phase conditions [42]—temperature $T = 1990$ K, pressure $P = 0.72$ bar, partial pressure of O_2 , $P_{O_2} = 8 \times 10^{-3}$ bar, ratio $P_{O_2}/P_{H_2} = 0.5$ —were used to calculate the initial concentrations of O_2 , H_2 , and Ar of the gaseous part of the model (Section 5.1). The initial PSDF moments were determined from the reported in [42] most probable diameter of the injected particles, $D_{pm} = 110$ nm, and their surface area, $a_p = 0.23$ cm²/cm³, with additional here assumptions of lognormal PSDF and its geometric standard deviation, $\sigma_g = 1.6$ (Section 5.2). The latter assumption was tested by varying σ_g from 1.1 to 2, and the results showed no measurable effect on properties of interest to the present analysis.

For the surface part of the reduced model (Section 5.3), the initial site number densities needed to be specified. In the present case, these are the properties of carbonaceous particles prepared elsewhere and injected into the shock tube prior to reaction. Without any pertinent details available, the following protocol was adopted. The reactive particle surface was assumed to be composed initially of only C_A -H and C_Z -H sites (with this assumption tested in Section 7), whose number densities were assigned through the initial values of α and ζ , namely,

$$\begin{aligned} \chi_{\text{nominal},0} &= \frac{\chi_s}{N_{Av}} a_p \\ [C_A - H]_0 &= (1 - \zeta_0)\alpha_0 \chi_{\text{nominal},0} \\ [C_Z - H]_0 &= \zeta_0 \alpha_0 \chi_{\text{nominal},0}, \end{aligned} \quad (47)$$

and α_0 and ζ_0 were assumed to be related by Eq. (38), namely, $\zeta_0 = 1 - 2\alpha_0$. Recalling that a_p is the experimentally determined initial particle surface area per cm³ (Section 4) leaves only α_0 unknown. Its value was determined by matching the experimental CO profile of the modeled experiment. The best match was found with $\alpha_0 = 0.27$. The results, depicted in the top-left panel Fig. 3, indicate that the model has the flexibility of predicting correctly the shape of the CO profile. This in itself is not a trivial outcome, considering the effort in attaining the same with a detailed stochastic model [2] and facing the high sensitivity to the fitted value, demonstrated by its 50 % changes yielding the dashed lines in the figure.

Also shown in Fig. 3 are number densities of surface sites (bottom left panel) and the corresponding values of surface-state descriptors, α and ζ (top right panel). As can be seen, the changes in these properties are small during the reaction time, thus validating, among other things, the neglect of pyrene in developing relationship (38). Likewise, the computed changes in particle ensemble properties, presented in Fig. 4, are relatively small, displaying about 10% decrease in particle mass and about 8% decrease in particle surface area, very close to the initial estimates (10 and 7%, respectively [2]), thus corroborating the assumed small degree of burnout in prior [2] and present model developments.

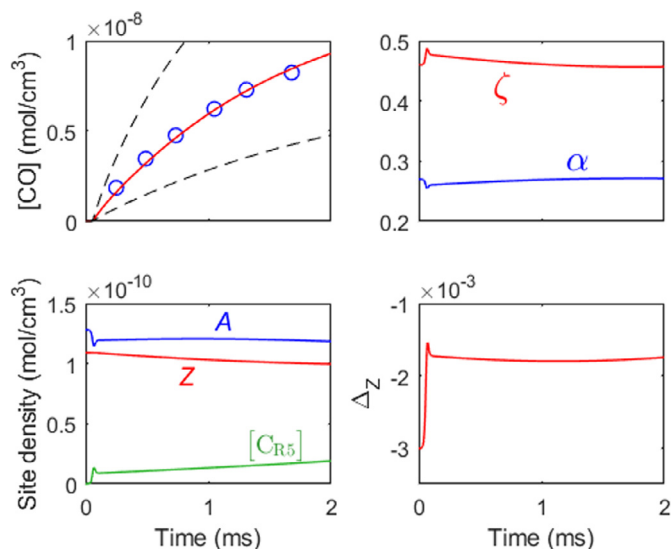


Fig. 3. Numerical results computed for the 1990K experiment of Roth et al. [42] with $\alpha_0 = 0.27$: top left, concentration of gaseous CO computed with $\alpha_0 = 0.27$ (red solid line), $\alpha_0 = 0.27 \times 1.5$ (upper dashed line), and $\alpha_0 = 0.27/1.5$ (lower dashed line), and experimental data (symbols) from Fig. 7 of Roth et al. [42]; top right, surface properties α and ζ , defined by Eqs. (33) and (37); bottom left: number densities of armchair, A (34), zigzag, Z (35), and embedded five-member-ring, C_{R5} , surface sites; bottom right, stoichiometric coefficient of zigzag products defined by Eq. (45). (For interpretation of the references to color in this figure legend, the reader is referred to the web version of this article.)

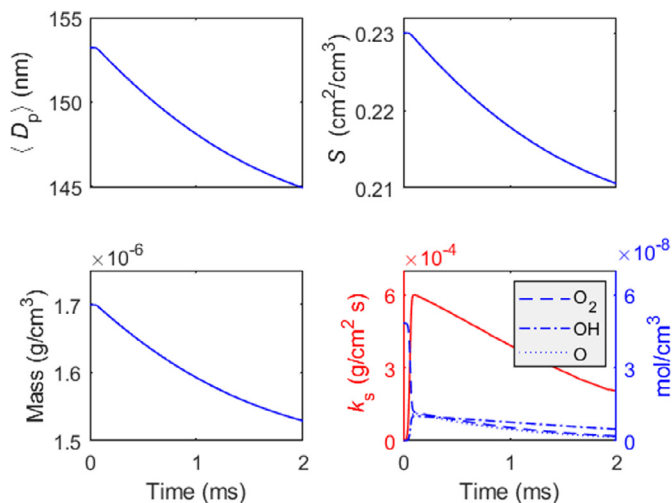


Fig. 4. Particle ensemble properties computed for the 1990K experiment of Roth et al. [42] with $\alpha_0 = 0.27$: top left, ensemble average particle diameter; top right, surface area per unit volume of the mixture; bottom left, carbon mass per unit volume in the mixture; bottom right, apparent oxidation rate “constant”, computed from Eq. (48) (red, left axis) and concentrations of oxidizers, O_2 , OH , and O (blue, right axis). (For interpretation of the references to color in this figure legend, the reader is referred to the web version of this article.)

The bottom-right panel of Fig. 4 displays the apparent oxidation rate “constant”, computed by summing up Eq. (18),

$$\sum_{i=1}^{\infty} \left(\frac{dm_i}{dt} N_i \right) = - \sum_{i=1}^{\infty} (k_s S_i N_i)$$

$$\frac{d \sum_{i=1}^{\infty} (m_i N_i)}{dt} = -k_s \sum_{i=1}^{\infty} (S_i N_i)$$

$$\frac{dM_1}{dt} = -k_s S, \quad (48)$$

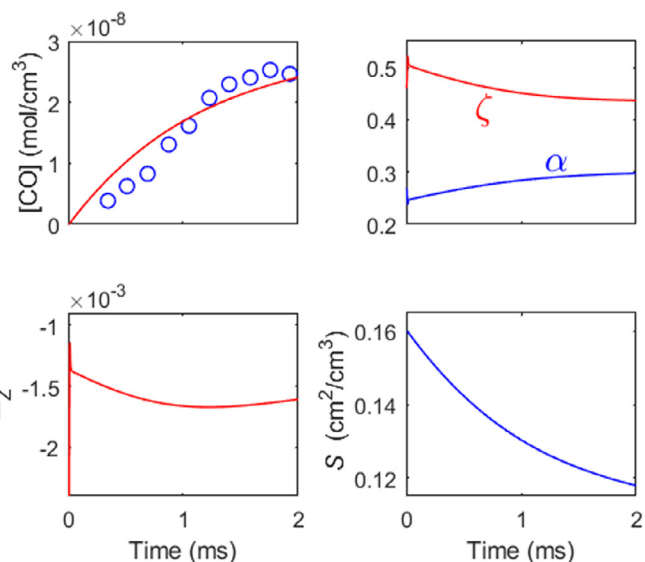


Fig. 5. Numerical results computed for the 2780K experiment of Roth et al. [42] with $\alpha_0 = 0.27$; the designation is the same as in Figs. 3 and 4; the experimental data points shown in the top left panel are from Fig. 4 of Roth et al. [42].

and solving for instantaneous k_s values from the resulting expression. The computed in this manner k_s first increases, due to rise in the gaseous radical pool and the corresponding increase in the surface radicals and hence oxyradicals, and then decreases, following the decay in the abundance of the oxidizers.

There is one more experiment of the H_2 - O_2 -Ar series, whose observed CO concentrations are reported in Roth et al.’s paper [42]. Its conditions, presented in Fig. 4 and Table 1 of [42], are: temperature $T = 2780$ K, pressure $P = 1.05$ bar, partial pressure of O_2 , $P_{O_2} = 1.25 \times 10^{-2}$ bar, ratio $P_{O_2}/P_{H_2} = 0.5$, and particle surface area, $a_p = 0.16$ cm^2/cm^3 . Numerical simulations with the present model of this experiment were performed using the same initial value of α as those of the 1990K experiment, namely, $\alpha_0 = 0.27$. The latter assignment follows from recognition that a quantifies the state of particle surface and, presumably, the same or similar carbonaceous particles were used in the course of the entire experimental series [42].

The numerical results are displayed in Fig. 5. The experimental values of the CO concentrations are reproduced by the model sufficiently close but the computed shape of the profile, as a whole, somewhat deviates from the experimental one. The difference could be due to a larger extent of oxidation at this high temperature, a 26% decrease in surface area, and larger variations in α and ζ . Yet, what is of most significance here is that the model, with its state-based treatment of surface chemistry, was able to reproduce two experiments, conducted at very different temperatures, without any adjustments and using the same initial value of α .

The latter outcome is further reiterated by numerical results obtained for the entire CO experimental series of Roth et al. [42]. The conditions of these experiments are presented in Table 1 of [42,77], listing the rates of CO production as observable results. Keeping the value of α_0 at 0.27, obtained for the 1990K experiment, the present model was applied to the entire set of experiments, ranging from 1652 to 3130 K. The computed rates for the comparison to the experimental values were obtained by fitting the 10–80 % parts of the computed CO profiles. The results, shown in Fig. 6, display a remarkable degree of agreement between experiment and model, considering that the same value of α_0 (i.e. no adjustments whatsoever in the model) was used over such a wide range of temperature.

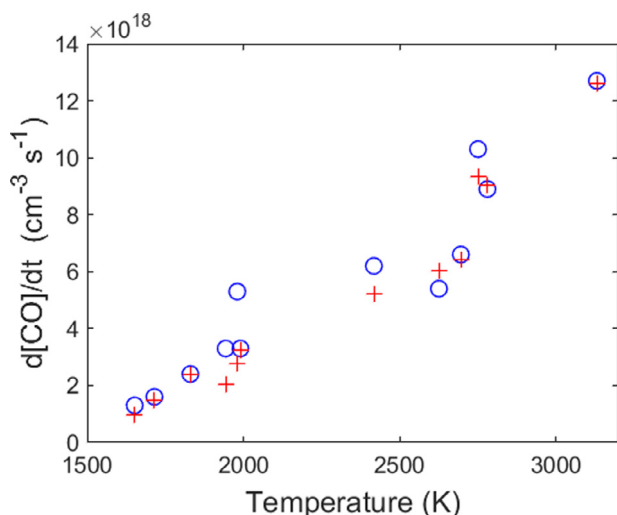


Fig. 6. Rate of CO production: blue circles, experimental data from Table 1 of Roth et al. [42, 77]; red pluses, computed with the present model using $\alpha_0 = 0.27$ for all the experimental runs. (For interpretation of the references to color in this figure legend, the reader is referred to the web version of this article.)

7. Sensitivity to the initial state of particle surface

In the numerical analysis described in Section 6, the initial state of the particle surface was assumed to be an ideal aromatic edge, composed only of proper six-member rings with all edge carbons saturated by hydrogen atoms. However, the carbonaceous particles introduced into the shock-tube experiments could have “processed” edges, considering the manufacturing process of the initial powder and subsequent treatment by the aerosol reactor of Roth et al. [43]. Indeed, Roth et al. [42] reported that the initial carbonaceous particles contained 0.4% hydrogen and 0.4% oxygen by mass. It is also known that carbon black may contain a similar amount of nitrogen [78]. Much less resolved is the detailed atomistic structure of particle surfaces, except that they contain carbon oxides [78] and can chemisorb water, oxygen, and nitrogen oxides [79].

Numerical tests were performed to probe the behavior of the new model form under differing assignments for the initial atomistic landscape of the particle surface. The first of them considered that the PAH constituents of the initial particle surface have all their armchair sites in the state of embedded five-member rings, i.e., all initial C_A -H sites replaced by half the amount of C_{R5} sites. Starting with such initial structure did not require refitting of α_0 and reproduced the CO concentrations similarly to the results reported in Figs. 3, 5, and 6. Decreasing, in addition, the fraction of the initial C_2 -H sites to attain the mass H/C ratio of 0.004 (e.g., by reduction of 80, 76, and 71% of the C_2 -H sites considering the geometries of $C_{54}H_{18}$, $C_{96}H_{24}$, and $C_{150}H_{30}$, respectively), produced no numerical differences in the computed CO profiles. Likewise, re-assignment of the initial distributions among armchair or among zigzag sites produced no noticeable differences in the numerical predictions of [CO]. At the same time, increasing the total number of C_A sites (either as C_A -H, C_A^* , C_A -O, or C_{R5}) by a factor 2, for instance, required reduction of α_0 to 0.19 to retain the same quality of fit for the CO concentrations in the validation tests.

The results of these sensitivity tests reiterate the rate-limiting role of the embedded five-member rings and demonstrate the robustness of the reduced model form in capturing this critical mechanistic feature identified in the detailed, sterically-resolved simulations [2].

8. Discussion

This section elaborates on the underlying features of the proposed model form. First, the surface reaction model moves away from the previously assumed steady state for surface radicals [14] and replaces it with gas-phase-like reaction kinetics. This, by itself, offers the flexibility of expressing the reaction mechanism at a desired level of complexity. The oxidation kinetics, addressed in the present study, required a multi-step representation to capture the key features of the mechanism identified in detailed modeling [2], which could not be expressed within the prior formalism.

While, in principle, there is no limit on the model size or form—which could be detailed, empirical, lumped, or a combination of such—the focus here is on developing a reduced formulation of surface processes to serve the needs of numerically-demanding computations. To accomplish this objective, the surface reaction model has to reproduce the steric features of the detailed mechanism. The present formulation achieves this by (a) introducing two state properties, α and ζ , and (b) postulating a relationship between them, $\zeta = 1 - 2\alpha$ (Eq. (38)), defined by and defining the structural evolution of the surface.

It is imperative to emphasize that while in the new model formulation α retains its initial definition, fraction of reactive sites of soot particle surface [14], it no longer serves as model “parameter”, which needs to be empirically parametrized, but becomes a surface state property. ζ , which accounts for the zigzag fraction of reactive sites, is a similar property. Both α and ζ represent and are determined by instantaneous surface site abundances. In the prior approach, α was parameterized in terms temperature and particle size (Section 2), where these properties were essentially used as surrogates of the reactive state of the surface; now this state is expressed directly, through surface inherent properties, α and ζ .

Introduction of α and ζ on its own does not produce new information, but simply summarizes the state of the surface, defined by instantaneous concentrations of individual surface sites. In fact, if the surface kinetic model included all reactions of all possible surface sites, expressing the detailed mechanism, no additional properties, like α and ζ , would be needed. The problem with such an approach would be an excessively large size of the model, required to capture the steric effects, i.e., all possible combinations of neighboring sites.

A reduced formulation that captures the steric constraints was accomplished by the introduced in Section 5.3 postulate. There are two key aspects of the postulate: structural and behavioral. The former is the apparent existence of a relationship between α and ζ for condensed aromatics, those that are expected to be the “islands of stability” of aromatic growth in combustion environments [19,20]. The behavioral side of the postulate is that the evolution of the surface during oxidation is assumed to follow this structural relationship, understood as averaged over and thus representing the entire particle surface. The postulate therefore suggests that the structural relationship, like Eq. (38), is purely geometric in nature, regardless of the sequence of reaction events and their kinetics, i.e., while the kinetics will possibly affect the order of reaction events, the α and ζ site fractions, on average, are mostly dependent on the carbon networking in the condense-PAH atomic structure.

Considering α and ζ as site fractions evaluated over the entire particle surface helps to explain the flexibility of the reduced model, as compared to the detailed model [2], in reproducing the shape of the experimental CO profile in Fig. 3. The detailed modeling [2] followed evolution of a single PAH substrate and showed a rapid decline in the oxidation rate that resulted in leveling off in the concentration profile of CO. This leveling off was explained by the formation of hard-to-oxidize embedded five member rings. The matching of the CO profile was attained by invoking

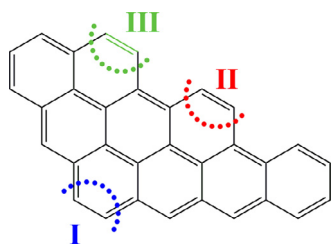


Fig. 7. Illustration of surface site reproduction.

multi-layer structure of the surface: as the oxidation of the top-layer PAH slows down and its periphery carbons are removed, the edges of the next-layer PAH become exposed to oxidation. In this way, both the top-layer and next-layer reactive sites constitute the total reactive-site coverage of the particle surface, and all these sites together define α and ζ of the reduced model. In other words, by following the ζ - α relationship and thus considering the overall surface coverage, the reduced model incorporates the multi-layer phenomenon of soot particle oxidation. The surface averaging also explains the relatively small changes in the computed values of α and, correspondingly, ζ , presented in Figs. 3 and 5; namely, while a single reaction event or a sequence of them for an individual PAH can deviate from the ζ - α relationship, on average, over time and surface, the relationship holds, with the net change in α balancing differing outcomes.

It is pertinent to emphasize that α is not entirely determined by the geometry of individual PAHs comprising the particle surface. α is defined (see Eq. 33) as the fraction of particle surface covered by reactive sites. The surface, however, may not necessarily be covered in its entirety by flat-laying PAHs but comprised, or parts of it, of overlapping PAHs thereby exposing reactive sites of multiple layers and of angled PAHs (as discussed in Section 2.2). The difference between the surface-site α , determined by surface site abundances, and the PAH-site α , computed from molecular PAH geometry, may reflect such surface structure.

We can now turn to the explanation of Reactions (S8) and (S9) of the mechanism (Table 1). Both are designed to reproduce the results of the detailed modeling study [2]. Reaction (S8) represents oxidative destruction of the embedded five-member rings, and it is rate-limiting. The reactants, rate coefficient, and rate law of Reaction (S8) are those of the detailed model, but its products are assigned varying stoichiometric coefficients, Δ_A and Δ_Z , thereby controlling the split between the armchair and zigzag sites. The physical picture of the reaction outcome is illustrated in Fig. 7. Consider the sites marked in Fig. 7 as I, II, and III. Each is an armchair site that can undergo H-abstraction, subsequent formation of an oxyradical, and its decomposition to gaseous CO and surface embedded five-member ring. The oxidation of the latter by O, reaction (S8), leaves behind two surface reactive sites, and hence the sum of Δ_A and Δ_Z must be equal to two, as stated by Eq. (39). However, depending on the particular steric environment of the reactant site, the product sites can be either both armchair (as in case I), both inner ‘zigzag’ (as in case II), or a mixture of the two (as in case III). Furthermore, the sites neighboring the products of I are ‘converted’ from inner zigzag to armchair as an additional outcome of Reaction (S8). The Δ_A and Δ_Z expressions, defined by Eqs. (45) and (46) and developed on the basis of the discussed above postulate, aim to account for the differing products of Reaction (S8). Considering the example cases in Fig. 7, it is somewhat surprising that the calculated value of the split, quantified by Δ_Z displayed in Figs. 3 and 5, is rather very small. This is, again, due to the surface averaging intrinsic to the ζ - α relationship, on which basis Δ_Z is developed. Another thing to notice is that such averaged value of Δ_Z can be either positive or negative.

Reaction (S9) designates thermal desorption of C_2H_2 , whose subsequent oxidation in the gas phase was seen in the detailed modeling [2] to contribute as much to CO production as the direct oxidation of surface sites. Therefore, the total rate of the latter was assigned to Reaction (S9). The detailed modeling also indicated that the formation of sites leading to C_2H_2 desorption usually originated with the removal of the embedded five-member rings, and this observation motivated the surface-site reactant assignment for Reaction (S9). Its surface-site products, left-behind chemisorbed C_2H_2 , and their stoichiometric coefficients were assumed to be the same as those of Reaction (S8).

Overall, the new surface model is congruent with the two-reactive-site empirical model discussed in Section 1, but with ‘more reactive sites’ of that model corresponding to those forming oxyradicals that decompose to CO and ‘less reactive sites’ to be the embedded five-member rings rather than ‘edge’ versus ‘basal’ sites [9]. Furthermore, in the present formulation, Reaction (S8) and (S9) combine the oxidation [4] and thermal [12] ‘steps’ of site transformation.

9. Conclusion

The introduced here new model form for the surface chemistry led to close reproduction of selected experimental data for soot oxidation, CO profiles in two experiments performed at substantially different temperatures, 1990 and 2780 K, as well as CO production rates over a wide range of temperatures, 1652–3130 K, all while fitting only the initial value of α . However, this fitting of α was done to determine the initial condition—reactive state of injected-particle surface. When particle inception and growth are included in the model, there will be no need for such a fitting, as the state of particle surface will be determined in a manner similar to the one described in the present work for the oxidation, from computed instantaneous site number densities. Such development and validation are the next endeavors. The present work introduces a model form that removes the empiricism remaining in the formulation of soot modeling and replaces it with a physics-based formalism.

References

- [1] B.S. Haynes, H.G. Wagner, The surface growth phenomenon in soot formation, *Z. Phys. Chem. N. F.* 133 (1982) 201–213.
- [2] M. Frenklach, Z. Liu, R.I. Singh, G.R. Galimova, V.N. Azyazov, A.M. Mebel, Detailed, sterically-resolved modeling of soot oxidation: role of O atoms, interplay with particle nanostructure, and emergence of inner particle burning, *Combust. Flame* 188 (2018) 284–306.
- [3] K.G. Neoh, J.B. Howard, A.F. Sarofim, Effect of oxidation on the physical structure of soot, *Symp. (Int.) Combust.* 20 (1985) 951–957.
- [4] J. Nagle, R.F. Strickland-Constable, Oxidation of carbon between 1000 and 2000 °C, Fifth Carbon Conference, Pergamon, Oxford (1962), pp. 154–164.
- [5] J. Appel, H. Bockhorn, M. Frenklach, Kinetic modeling of soot formation with detailed chemistry and physics: laminar premixed flames of C_2 hydrocarbons, *Combust. Flame* 121 (2000) 122–136.
- [6] T.F.E. Rhead, R.V. Wheeler, LIII.—The mode of combustion of carbon, *J. Chem. Soc. Trans.* 103 (1913) 461–489.
- [7] I. Langmuir, Chemical reactions at low pressures, *J. Am. Chem. Soc.* 37 (1915) 1139–1167.
- [8] C.J. Tighe, M.V. Twigg, A.N. Hayhurst, J.S. Dennis, The kinetics of oxidation of Diesel soots and a carbon black (Printex U) by O_2 with reference to changes in both size and internal structure of the spherules during burnout, *Carbon* 107 (2016) 20–35.
- [9] C.K. Gaddam, R.L. Vander Wal, X. Chen, A. Yezerets, K. Kamasamudram, Reconciliation of carbon oxidation rates and activation energies based on changing nanostructure, *Carbon* 98 (2016) 545–556.
- [10] R.F. Strickland-Constable, The interaction of oxygen and carbon filaments at high temperatures, *Trans. Faraday Soc.* 40 (1944) 333.
- [11] R. Phillips, F.J. Vastola, P.L. Walker, Factors affecting the product ratio of the carbon-oxygen reaction—II. Reaction temperature, *Carbon* 8 (1970) 205–210.
- [12] A.M. Nienow, J.T. Roberts, M.R. Zachariah, Surface chemistry of nanometer-sized aerosol particles: reactions of molecular oxygen with 30 nm soot particles as a function of oxygen partial pressure, *J. Phys. Chem. B* 109 (2005) 5561–5568.

- [13] M. Frenklach, Soot formation in combustion: an international round table discussion, Göttingen, 1989, pp. 35–36.
- [14] M. Frenklach, H. Wang, Detailed modeling of soot particle nucleation and growth, *Symp. (Int.) Combust.* 23 (1991) 1559–1566.
- [15] K.G. Neoh, J.B. Howard, A.F. Sarofim, Soot oxidation in flames, in: D.C. Siegla, G.W. Smith (Eds.), *Particulate carbon: formation during combustion*, Plenum, New York, 1981, pp. 261–282.
- [16] A. Veshkini, S.B. Dworkin, M.J. Thomson, A soot particle surface reactivity model applied to a wide range of laminar ethylene/air flames, *Combust. Flame* 161 (2014) 3191–3200.
- [17] A. Khosousi, S.B. Dworkin, Soot surface reactivity during surface growth and oxidation in laminar diffusion flames, *Combust. Flame* 162 (2015) 4523–4532.
- [18] A. Khosousi, S.B. Dworkin, Detailed modelling of soot oxidation by O₂ and OH in laminar diffusion flames, *Proc. Combust. Inst.* 35 (2015) 1903–1910.
- [19] M. Frenklach, D.W. Clary, W.C. Gardiner Jr, S.E. Stein, Detailed kinetic modeling of soot formation in shock-tube pyrolysis of acetylene, *Symp. (Int.) Combust.* 20 (1985) 887–901.
- [20] M. Frenklach, Reaction mechanism of soot formation in flames, *Phys. Chem. Chem. Phys.* 4 (2002) 2028–2037.
- [21] M. Frenklach, On surface growth mechanism of soot particles, *Symp. (Int.) Combust.* 26 (1996) 2285–2293.
- [22] M. Frenklach, Computer modeling of infinite reaction sequences: a chemical lumping, *Chem. Eng. Sci.* 40 (1985) 1843–1849.
- [23] M. Frenklach, S.J. Harris, Aerosol dynamics modeling using the method of moments, *J. Colloid Interface Sci.* 118 (1987) 252–261.
- [24] M. Frenklach, H. Wang, Detailed mechanism and modeling of soot particle formation, in: H. Bockhorn (Ed.), *Soot formation in combustion: mechanisms and models*, Springer-Verlag, Heidelberg, 1994, pp. 165–192.
- [25] R. Vander Wal, A. Yezerets, N.W. Currier, D.H. Kim, C.M. Wang, HRTEM study of diesel soot collected from diesel particulate filters, *Carbon* 45 (2007) 70–77.
- [26] B. Rohani, C. Bae, Morphology and nano-structure of soot in diesel spray and in engine exhaust, *Fuel* 203 (2017) 47–56.
- [27] F.A. Heckman, D.F. Harling, Progressive oxidation of selected particles of carbon black: further evidence for a new microstructural model, *Rubber Chem. Technol.* 39 (1966) 1–13.
- [28] H.B. Palmer, C.F. Cullis, The formation of carbon from gases., in: P.L. Walker (Ed.), *Chemistry and Physics of Carbon*, Marcel Dekker, New York, 1965, pp. 265–325.
- [29] J. Lahaye, G. Prado, Morphology and internal structure of soot and carbon blacks, in: D.C. Siegla, G.W. Smith (Eds.), *Particulate Carbon. Formation During Combustion*, Plenum, New York, 1981, pp. 33–55.
- [30] B.S. Haynes, H.G. Wagner, Soot formation, *Prog. Energy Combust. Sci.* 7 (1981) 229–273.
- [31] A. Kazakov, H. Wang, M. Frenklach, Detailed modeling of soot formation in laminar premixed ethylene flames at a pressure of 10 bar, *Combust. Flame* 100 (1995) 111–120.
- [32] R. Whitesides, M. Frenklach, Detailed kinetic Monte Carlo simulations of graphene-edge growth, *J. Phys. Chem. A* 114 (2010) 689–703.
- [33] M. Balthasar, M. Frenklach, Detailed kinetic modeling of soot aggregate formation in laminar premixed flames, *Combust. Flame* 140 (2005) 130–145.
- [34] J. Singh, M. Balthasar, M. Kraft, W. Wagner, Stochastic modeling of soot particle size and age distributions in laminar premixed flames, *Proc. Combust. Inst.* 30 (2005) 1457–1465.
- [35] S.B. Dworkin, Q. Zhang, M.J. Thomson, N.A. Slavinskaya, U. Riedel, Application of an enhanced PAH growth model to soot formation in a laminar coflow ethylene/air diffusion flame, *Combust. Flame* 158 (2011) 1682–1695.
- [36] H. Jander, *Personal communication*, 1992.
- [37] J.Y.W. Lai, P. Elvati, A. Violi, Stochastic atomistic simulation of polycyclic aromatic hydrocarbon growth in combustion, *Phys. Chem. Chem. Phys.* 16 (2014) 7969–7979.
- [38] E.K.Y. Yapp, C.G. Wells, J. Akroyd, S. Mosbach, R. Xu, M. Kraft, Modelling PAH curvature in laminar premixed flames using a detailed population balance model, *Combust. Flame* 176 (2017) 172–180.
- [39] D.T. Gillespie, *Markov processes: an introduction for physical scientists*, Academic Press, San Diego, CA, 1992.
- [40] M. Frenklach, Monte Carlo simulation of diamond growth by methyl and acetylene reactions, *J. Chem. Phys.* 97 (1992) 5794–5802.
- [41] J.I. Steinfeld, J.S. Francisco, W.L. Hase, *Chemical kinetics and dynamics*, Prentice Hall, Upper Saddle River, N. J., 1999.
- [42] P. Roth, O. Brandt, S. Von Gersum, High temperature oxidation of suspended soot particles verified by CO and CO₂ measurements, *Symp. (Int.) Combust.* 23 (1991) 1485–1491.
- [43] O. Brandt, A.M. Rajathurai, P. Roth, First observations on break-up of particle agglomerates in shock waves, *Exp. Fluids* 5 (1987) 86–94.
- [44] D. Rivin, A.I. Medlia, A comparative study of soot and carbon black, in: J. Lahaye, G. Prado (Eds.), *Soot in Combustion Systems and its Toxic Properties*, Plenum, New York, 1983, pp. 25–35.
- [45] A.N. Watson, P.A. Valberg, Carbon black and soot: two different substances, *Am. Ind. Hyg. Assoc. J.* 62 (2001) 218–228.
- [46] R.L. Vander Wal, A TEM methodology for the study of soot particle structure, *Combust. Sci. Technol.* 126 (1997) 333–351.
- [47] Á.B. Palotás, L.C. Rainey, C.J. Feldermann, A.F. Sarofim, J.B. Vander Sande, Soot morphology, An application of image analysis in high-resolution transmission electron microscopy, *Microsc. Res. Tech.* 33 (1996) 266–278.
- [48] B.R. Stanmore, J.F. Brilhac, P. Gilot, The oxidation of soot: a review of experiments, mechanisms and models, *Carbon* 39 (2001) 2247–2268.
- [49] M. Balthasar, F. Mauss, A. Knobel, M. Kraft, Detailed modeling of soot formation in a partially stirred plug flow reactor, *Combust. Flame* 128 (2002) 395–409.
- [50] R. Taylor, Orion engineering carbons, LLC. *Personal communication*, 2018.
- [51] S.K. Friedlander, *Smoke, dust, and haze: fundamentals of aerosol dynamics*, Oxford University, Oxford, UK, 2000.
- [52] D.J. Strom, P.S. Stansbury, Determining parameters of lognormal distributions from minimal information, *Am. Ind. Hyg. Assoc. J.* 61 (2000) 877–880.
- [53] P.J. DeMott, Y. Chen, S.M. Kreidenweis, D.C. Rogers, D.E. Sherman, Ice formation by black carbon particles, *Geophys. Res. Lett.* 26 (1999) 2429–2432.
- [54] O. Möhler, S. Büttner, C. Linke, M. Schnaiter, H. Saathoff, O. Stetzer, R. Wagner, M. Krämer, A. Mangold, V. Ebert, U. Schurath, Effect of sulfuric acid coating on heterogeneous ice nucleation by soot aerosol particles, *J. Geophys. Res. Atmos.* 110 (2005) D11.
- [55] X. You, A. Packard, M. Frenklach, Process Informatics tools for predictive modeling: hydrogen combustion, *Int. J. Chem. Kinet.* 44 (2012) 101–116.
- [56] *PrIme Warehouse*. <http://warehouse.cki-know.org/depository/models/catalog/m00000004.xml> (accessed September 2018).
- [57] D.L. Baulch, C.T. Bowman, C.J. Cobos, R.A. Cox, T. Just, J.A. Kerr, M.J. Pilling, D. Stocker, J. Troe, W. Tsang, R.W. Walker, J. Warnatz, Evaluated kinetic data for combustion modeling: supplement II, *J. Phys. Chem. Ref. Data* 34 (2005) 757–1397.
- [58] M. Frenklach, Dynamics of discrete distribution for Smoluchowski coagulation model, *J. Colloid Interface Sci.* 108 (1985) 237–242.
- [59] A. Kazakov, M. Frenklach, Dynamic modeling of soot particle coagulation and aggregation: implementation with the method of moments and application to high-pressure laminar premixed flames, *Combust. Flame* 114 (1998) 484–510.
- [60] M. Frenklach, Method of moments with interpolative closure, *Chem. Eng. Sci.* 57 (2002) 2229–2239.
- [61] H.M. Hulburt, S. Katz, Some problems in particle technology. A statistical mechanical formulation, *Chem. Eng. Sci.* 19 (1964) 555–574.
- [62] R. Singh, M. Frenklach, A mechanistic study of the influence of graphene curvature on the rate of high-temperature oxidation by molecular oxygen, *Carbon* 101 (2016) 203–212.
- [63] A.S. Semenkikh, A.S. Savchenkova, I.V. Chechet, S.G. Matveev, Z. Liu, M. Frenklach, A.M. Mebel, Rate constants for H abstraction from benzo(a)pyrene and chrysene: a theoretical study, *Phys. Chem. Chem. Phys.* 19 (2017) 25401–25413.
- [64] L.B. Harding, Y. Georgievskii, S.J. Klippenstein, Predictive theory for hydrogen atom–Hydrocarbon radical association kinetics, *J. Phys. Chem. A* 109 (2005) 4646–4656.
- [65] V.V. Kislov, R.I. Singh, D.E. Edwards, A.M. Mebel, M. Frenklach, Rate coefficients and product branching ratios for the oxidation of phenyl and naphthyl radicals: a theoretical RRKM-ME study, *Proc. Combust. Inst.* 35 (2015) 1861–1869.
- [66] R.I. Singh, Development and implementation of detailed soot surface oxidation model into kinetic monte carlo simulations of graphene-edge oxidation Ph.D. Thesis, University of California, Berkeley, 2016.
- [67] Jr D.E. Edwards, X. You, D.Y. Zubarev, W.A. Lester, M. Frenklach, Thermal decomposition of graphene armchair oxyradicals, *Proc. Combust. Inst.* 34 (2013) 1759–1766.
- [68] T. Seta, M. Nakajima, A. Miyoshi, High-temperature reactions of OH radicals with benzene and toluene, *J. Phys. Chem. A* 110 (2006) 5081–5090.
- [69] D.E. Edwards, D.Y. Zubarev, W.A. Lester, M. Frenklach, Pathways to soot oxidation: reaction of OH with phenanthrene radicals, *J. Phys. Chem. A* 118 (2014) 8606–8613.
- [70] H.I. Leidreiter, H.G. Wagner, An investigation of the reaction between O(3P) and benzene at high temperatures, *Z. Phys. Chem. N. F.* 165 (1989) 1–7.
- [71] R.I. Singh, A.M. Mebel, M. Frenklach, Oxidation of graphene-edge six- and five-member rings by molecular oxygen, *J. Phys. Chem. A* 119 (2015) 7528–7547.
- [72] Y. Hidaka, T. Oki, H. Kawano, T. Higashihara, Thermal decomposition of methanol in shock waves, *J. Phys. Chem.* 93 (1989) 7134–7139.
- [73] X. You, D.Y. Zubarev, W.A. Lester Jr, M. Frenklach, Thermal decomposition of pentacene oxyradicals, *J. Phys. Chem. A* 115 (2011) 14184–14190.
- [74] *Matlab*. <http://www.mathworks.com/>.
- [75] E. Goos, A. Burcat, B. Ruscic, Extended third millennium deal gas thermochemical database with updates from active thermochemical tables. <http://burcat.technion.ac.il/dir> (accessed June 2018).
- [76] H. Kellerer, R. Koch, S. Wittig, Measurements of the growth and coagulation of soot particles in a high-pressure shock tube, *Combust. Flame* 120 (2000) 188–199.
- [77] Apparently, There is typo in Table 7 of Roth et al. [38]. The values listed in the third column of the CO series should be ten times larger. This conclusion can be reached by (a) comparing the value of P_{O₂} listed in Fig. 4 and the corresponding entry for the same experiment in Table 7, and (b) performing calculations of the H₂–O₂ system presented in Fig. 7 and comparing the corresponding species concentrations.
- [78] What is Carbon Black? <https://www.thecarycompany.com/media/pdf/specs/orion-what-is-carbon-black.pdf>.
- [79] C. Alcalá-Jornod, H. van den Bergh, M.J. Rossi, Reactivity of NO₂ and H₂O on soot generated in the laboratory: a diffusion tube study at ambient temperature, *Phys. Chem. Chem. Phys.* 2 (2000) 5584–5593.